Heat-Shield Ablation at Superorbital Re-Entry Velocities

E. P. BARTLETT* AND W. E. NICOLET†
Aerotherm Corporation, Mountain View, Calif.

AND

J. T. HOWE‡
NASA Ames Research Center, Moffett Field, Calif.

Solutions are presented for the ablation of various heat-shield materials subjected to superorbital re-entry conditions. Convective heating rates are determined by coupled solution of the chemically-reacting boundary-layer equations and the surface ablation response, while satisfying surface equilibrium and steady-state energy balances. Incident radiation, treated parametrically, is permitted to pass unattenuated through the boundary layer. Emphasis is paid to graphite and nylon-phenolic at flight velocities of 35,000–55,000 fps, and nose radius R_N is varied to cover the range from convection-dominated flows (small R_N) to zero-convective-heating flows (large R_N). The results demonstrate that doubling of the total (convective plus radiative) heating rate can produce a sixfold increase in ablation rate. Consequently, vehicle sizing should be based upon ablation-rate rather than total-heating considerations. The R_N for minimum ablation depends strongly upon the assumed radiative flux to the surface as well as upon the material and trajectory.

Nomenclature

B' = blowing parameter, $\dot{m}_w/\rho_e u_e C_M$
B_0' = blowing parameter, $\dot{m}_w/\rho_e u_e C_{H_0}$
C_H = heat-transfer coefficient; C_{H_0} applies for a nonablating wall at the ablation temperature
C_M = mass-transfer coefficient; C_{M_k} for element k
F_c = reduction in incident radiation flux due to nonadiabatic effects
h = gas static enthalpy, Btu/lb; h_w at wall
h_∞ = altitude, kft
H = total enthalpy, Btu/lb
j_k = diffusional mass flux of element k, lb/sec-ft²
$\tilde{K}_k$ = mass fraction of element k irrespective of molecular configuration
$\dot{m}_w$ = surface ablation rate, lb/sec-ft²
P = pressure, atm
q_a = convective heat transfer, Btu/sec-ft²
q_r = radiation flux, Btu/sec ft²; q_{rad}, from an adiabatic layer
q_{rerad} = energy reradiated from the surface, Btu/sec-ft²
q_R = baseline incident radiation flux, Btu/sec-ft²
R_N = nose radius, ft
T = temperature, °R
u_e = boundary-layer edge velocity, fps
V_∞ = freestream velocity, fps
Γ = radiation cooling parameter
δ = shock standoff distance, ft
$\delta\dot{\nu}$ = frequency increment small compared to the span of a molecular band system but large compared to an individual band, ev
ϵ = density ratio across bow shock
ϵ_w = surface emittance
$\bar{\mu}_{\dot{\nu}}$ = molecular band absorption coefficient obtained from bandless model approximation, cm^{-1}
$\mu_{\dot{\nu}}$ = detailed absorption coefficient of molecular band system, calculated using the just-overlapping line approach, cm^{-1}
ρ = density, lb/ft³

Subscripts

e = boundary-layer edge
k = element
0 = nonablating
s = stagnation
v = virgin material
w = wall

Presented as Paper 70-202 at the AIAA 8th Aerospace Sciences Meeting, New York, January 19–21, 1970; submitted May 4, 1970; revision received December 21, 1970. This work was supported by NASA/Headquarters under Contract NASW-1749.

* Manager, Applied Research Department. Member AIAA.
† Staff Engineer, Applied Research Department. Member AIAA.
‡ Research Scientist.

Introduction

THE calculation of heat-shield ablation rate $\dot{m}_w$ during superorbital re-entry requires knowledge of the material properties, the radiative and convective heating rates q_r and q_a, the wall temperature T_w, the enthalpy of the gas at the wall h_w, the energy stored due to transient conduction, and the pyrolysis gas rate. In order to avoid estimating any of these quantities, it would be necessary to couple a radiation-coupled viscous shock-layer procedure to a transient charring-ablation conduction procedure. Some of the more important requirements of such a computational procedure are that the shock-layer species equations should be solved considering all potentially important chemical reactions, a nongray radiation model including line transitions and contributions from ablation products, and surface equilibrium (or rate chemistry) and energy and mass balances at the surface. Such a coupled code does not exist, and if it did, it would be too expensive to use in support of heat-shield design studies. Therefore, it is necessary to perform a certain amount of decoupling and/or to make idealizations and approximations to obtain the necessary information. The problem has typically been decoupled at the surface with attention being directed either to the ablation problem or to the radiation-coupled shock-layer problem.

The conventional approach[1,2] has been to concentrate on in-depth material response and a surface thermochemical boundary condition,[3] while employing correlations for q_r and approximating q_a by nonablating heat-transfer coefficients modified by blowing corrections. Obviously, this approach does not permit detailed consideration of radiation-convection coupling, but such effects can be treated approximately by applying corrections based on correlations of partially decoupled solutions.

Anderson's survey[4] shows that radiation-coupled shock-layer solutions generated during the last several years differ mainly in the nature of the radiation properties models employed. Only the more recent studies[5-9] are of practical interest, since earlier studies used radiation properties models which are now judged to be in substantial error. Typically, these studies have either neglected mass addition or have treated surface mass transfer parametrically (i.e., assigned injection rates) without consideration of surface equilibrium or a surface energy balance. Thus, while correlations of these solutions are useful as input for decoupled ablation calculations such as those described in the previous paragraph, they do not constitute ablation studies in themselves.

This paper presents solutions for the chemically-reacting stagnation-point boundary layer fully coupled to a steady-state ablation boundary condition. The incident q_r is considered to pass through the boundary layer without altering boundary-layer profiles directly; the boundary-layer profiles are affected indirectly, however, through the pronounced effect of the incident radiation on the surface energy balance and, consequently, on $\dot{m}_w$. The surface is considered to be in equilibrium with the gas adjacent to it; $\dot{m}_w$, q_a, and T_w are obtained during the course of the calculation, while the pyrolysis gas rate is a fixed fraction of $\dot{m}_w$ and the storage term is zero due to the steady-state approximation.

The steady-state assumption eliminates the need for coupling to a finite-difference charring-ablation solution procedure. Steady state tends to be a good approximation for the severe flight conditions associated with interplanetary return velocities. Nevertheless, the results are correlated and presented such that they can be used to perform transient ablation predictions when transient effects are deemed important.

The radiation flux incident to the surface is treated as a parameter of the problem. Consequently, the results are independent of any radiation properties model, and new models can be employed as they become available. The baseline radiation heating rates (q_R's) employed are based on solutions for self-absorbing, isothermal adiabatic shock layers corrected for radiation cooling using a correlation proposed by Olstad.[10] These solutions were generated using a nongray radiation model including lines.[11] A second flux is taken to be $q_R/2$ for each condition considered. The use of this factor is consistent with the results of studies[2,4,12] which predict that incident heating rates can be reduced by a factor of two or more by ablation products absorption.

Solutions are presented for a range of nose radii for graphite, nylon-phenolic, the Apollo material, and teflon with emphasis on the former two materials. Velocities of 35–55 kft/sec and altitudes of 190 and 220 kft are considered. Procedures are described by which these results can be used to obtain ablation predictions for particular configurations and trajectories. Finally, implications of the results with regard to the sizing of re-entry heat shields are discussed.

Analytical Approach

In the absence of mechanical removal effects, the energy balance at the wall can be expressed in the steady-state limit as

$$\dot{m}_w h_v - \dot{m}_w h_w + q_{a_w} + q_{r_w} - q_{\text{rerad}} = 0 \qquad (1)$$

where h_v and h_w are the enthalpies of the undisturbed virgin material and the gaseous mixture at the wall, q_{a_w} is the convective heat transfer to the surface (conduction plus diffusion), q_{r_w} is the radiative heat flux absorbed by the wall, and q_{rerad} is the energy reradiated from the wall. In the present study q_{a_w} is obtained by solution of the boundary-layer equations with a coupled surface ablation boundary condition, and T_w and the composition of the gas at the wall (and hence q_{rerad} and h_w) are also obtained in the solution. The q_{r_w} is computed a priori and considered as input to the boundary-layer solution.

Table 1 Material properties

Composition, wt %	Graphite	Nylon-phenolic
C	100.0	70.20
H	...	8.15
N	...	6.15
O	...	15.50
Surface absorptivity	1.00	1.00
Surface emittance	1.00	0.65
Heat of formation at 298°K, Btu/lb	0	−1311
Material density, lb/ft³	115	75

Boundary-Layer Solution Procedure

The boundary-layer solutions were generated using a detailed numerical solution procedure[13,14] which is capable in the limit of yielding exact solutions to the equations which are solved.§ Enough nodes are employed herein that numerical inaccuracies probably seldom exceed 1% in quantities of engineering interest. The boundary layer is considered to be in equilibrium, the evaluation of the chemical state being fully coupled with the governing conservation equations with nominally 30–40 species given consideration. The thermodynamic properties for the species considered are computed from curve fits[17] of JANAF and other reliable data. Mixture viscosity and thermal conductivity are computed from approximate relations of the Wilke type.[17,18] (Species viscosity and diffusion coefficient data used in these relations are summarized in Ref. 17.) Diffusive fluxes are calculated considering equal binary diffusion coefficients employing the concept of an effective diffusion coefficient.[3,17]

The ablating surface is considered to be in equilibrium with the boundary-layer gases adjacent to it for all materials except teflon, for which a rate law relating $\dot{m}_w$ to T_w is employed. The wall boundary condition is completed by consideration of elemental mass balances and a steady-state energy balance. The compositions, surface absorptivities and emittances, heats of formation, and densities employed for graphite and nylon-phenolic are presented in Table 1. The properties employed for teflon and the Apollo material are presented in Ref. 19.

A novel numerical solution procedure, termed an "integral-matrix" approach,[13,14] has proven to be economical and to have excellent convergence characteristics even for the highly-blown, chemically-reacting, ablation-coupled boundary layers of the present study. It utilizes general Newton-Raphson iteration to solve the set of nonlinear algebraic equations which results from the use of quadratic spline interpolation functions and the use of integration across the boundary layer with step weighting functions. Convergence is controlled by an elaborate damping scheme which restricts the size of corrections permitted for the current iteration.

Even for massive blowing, the boundary-layer equations are solved all the way to the wall, thus circumventing the need for matching of an inviscid inner layer and a viscous outer layer, for example. For very large blowing rates, an isothermal layer of ablation products, while not assumed, is predicted to exist adjacent to the wall, as illustrated in Fig. 1

§ This procedure has been automated to apply to a general class of problems. While the present study is limited to the stagnation-point chemically-reacting boundary layer with assumed equal diffusion coefficients, the procedure applies to the nonsimilar laminar/turbulent multicomponent boundary layer.[14,15] Solutions have also been obtained with a coupled transient charring ablation wall boundary condition[15,16] and while considering coupled radiation absorption (including ablation products) using a nongray radiation model (including lines).[16]

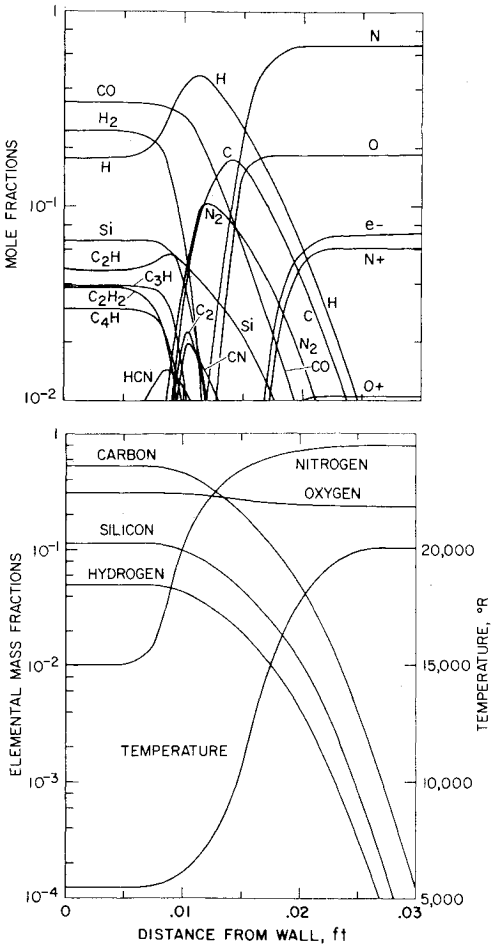

Fig. 1 Typical boundary-layer profiles over the Apollo material for a very high ablation rate.

The isothermal layer of ablation products is roughly the same thickness as the mixing layer in this particular problem and consists of primarily CO, H_2, H, and Si with some C_2H, C_3H, C_2H_2, and C_4H. In the mixing region, the dominant species become H, CO, C, and N_2 with the appearance of some C_2, CN, and HCN. Finally, as the boundary-layer edge is approached, the ablation products disappear and dissociated partially ionized air prevails.

Whereas some solutions for blown-off boundary layers such as the above example were obtained during the course of the study, ablation rates under these conditions were typically calculated directly from Eq. (1) with $q_{a_w} = 0$ and q_{rerad} and h_w calculated from the material sublimation temperature and composition.

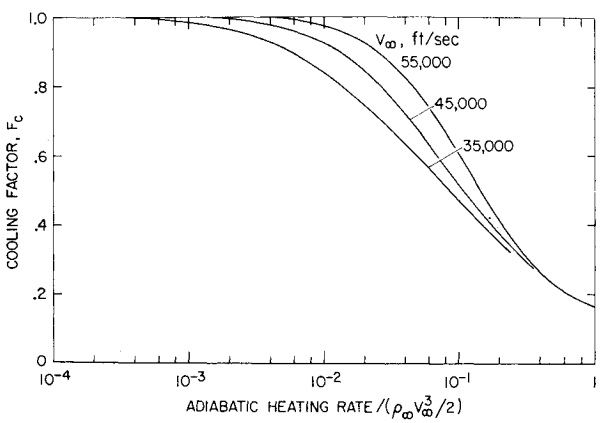

Fig. 2 Radiation cooling factor.

Baseline Radiation Calculation

The baseline radiation calculations were performed in four steps. Initially, the standoff distance and thermodynamic state of the shock layer were obtained while requiring it to be adiabatic. Then, the radiation properties and transport models of Nicolet[11] were employed to obtain adiabatic layer fluxes. Finally, the correlations of Olstad[10] were used to correct the adiabatic layer fluxes to account for radiation cooling.

The thermodynamic states across the layer were taken equal to those just behind the bow shock wave, in accordance with the strong-shock-wave approximation. These were calculated for the flight conditions of interest by solution of the jump conditions subject to the requirements of chemical equilibrium.[20] The standoff distance follows immediately from the relation

$$\delta = R_N\epsilon/[1 + (8\epsilon/3)^{1/2}] \qquad (2)$$

which is accurate for spheres in the strong-shock limit.[21] Representative values of the standoff distances and thermodynamic states used in the present study are presented in Table 2.

A detailed (rather than multistep) properties model[11] was employed which includes individual contributions from molecular band systems, continuum transitions, and atomic and ionic lines. The contribution from each of the molecular systems is calculated using the bandless model, viz.

$$\bar{\mu}_\nu = [\int_{\delta\dot{\nu}} \mu_\nu d\nu]/\delta\dot{\nu} \qquad (3)$$

which retains the essential features of the band system while significantly reducing the amount of data required for its characterization. The μ_ν values for the molecular band systems are taken from Woodward,[22] Biberman and Mnatsakanyan,[23] and other reliable sources. The 1+, 2+, and Birge-Hopfield band systems are used for N_2; the Schumann-Runge for O_2; the γ, β, δ and ϵ for NO; and the 1- for N_2^+.

Contributions are included for the continuum transitions associated with photodissociation (O_2), photoionization (NO, N, O, N^+ and O^+), photodetachment (O^-) and free-free ($N^+ - e$ and $O^+ - e$). No N^- contribution was included,¶ but since N^- radiates in the optically thin region of the spectrum, its contribution could be added after the fact, if desired.

Finally, contributions were included for the high lines** (N,O), the high series (N,O) and for each of 118 low lying lines (N, O, N^+, O^+). Lorentz and Doppler line shapes were allowed with the (half) half width calculation including the Stark, resonance, and Doppler effects. At a particular frequency, the line contribution was approximated by summing over only the nearby lines and neglecting the distant ones in accordance with the line group approximation. This pro-

Table 2 Shock layer conditions

Altitude, kft	Flight velocity, fps	State properties		
		P_s, atm	H_s, Btu/lb	T_s, °R
220	35,000	0.1357	24,376	18,758
220	45,000	0.2253	40,318	22,906
220	55,000	0.3368	60,234	26,947
190	35,000	0.4151	24,368	19,740
190	45,000	0.6890	40,302	24,489
190	55,000	1.0299	60,209	28,977

¶ The magnitude of the N^- contribution (if any) is quite uncertain.

** The high lines have upper principal quantum numbers of 8 or greater. The high series have lower principal quantum numbers of 4 or greater.

cedure simplifies the calculation while retaining the essential features of line overlapping.

The radiation transport model[11] considers the nongray, self-absorbing flux associated with a plane-parallel slab. The resulting transport integrals have been simplified slightly by employing the exponential approximation, but are otherwise completely general. The transport integrals are evaluated numerically with careful attention to the selection of nodal points (in frequency and space) and interpolation functions to insure that high accuracy is maintained.

The adiabatic layer fluxes were calculated for the three velocities and two altitudes shown in Table 2 for body radii ranging from 0.001 to 20 ft. A representative selection of the results is presented in Table 3. The contributions from the continuum (including molecular band systems) and from the lines are also shown in Table 3. The line contributions dominate the total flux for the smallest R_N shown, but the line and continuum contributions are of roughly equal importance for the largest R_N.

The radiation cooling factors of Olstad, presented in Fig. 2 as functions of the radiation cooling parameter $\Gamma \equiv q_{rad}/(\rho_\infty V_\infty^3/2)$, were used to obtain the corrected baseline fluxes q_R given in Fig. 3.

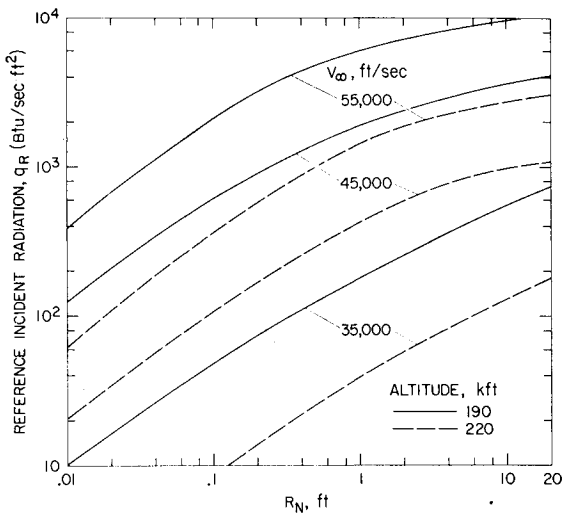

Fig. 3 Reference incident radiation heating rates.

Results

Solutions were obtained for graphite, nylon-phenolic, the Apollo material, and teflon, for the baseline q_R (see Fig. 3) and for $q_R/2$; solutions were obtained over large ranges of R_N from convection-dominated (small R_N) to radiation-dominated flows. In the present paper only the graphite and nylon-phenolic ablation-rate results and correlations of q_{a_w} are presented in detail. A comprehensive presentation of results for all four materials, including T_w and h_w, can be found in Ref. 19.

Ablation Rates

Figures 4 and 5 present $\dot{m}_w$ vs log R_N for graphite and nylon-phenolic, respectively (at different flight velocities), for two altitudes, and for q_R and $q_R/2$. The results for the baseline heating rate q_R are representative of solutions which neglect the effect of ablation-products absorption on q_{r_w}, while the $q_R/2$ results might be considered as representative of solutions which include this effect.

The solutions for q_R show fairly pronounced minima in $\dot{m}_w$ at the lower altitude (190 kft) for all flight velocities and materials considered. These minima tend to become more sharply defined and to occur at smaller R_N as $\dot{m}_w$ is increased due either to a higher V_∞ or a less efficient ablator (graphite being the most efficient). For nylon-phenolic, the R_N for minimum $\dot{m}_w$ decreases from 5.0 to 0.12 ft as $\dot{m}_w$ is increased from 0.012 to 0.23 lb/sec-ft^2 in going from the least severe case (35 kft/sec) to the most severe case (55 kft/sec). At the higher altitude, the range of R_N for minimal $\dot{m}_w$ is much broader, especially for nylon-phenolic at 35 kft/sec and graphite at 45 kft/sec. In these cases the minimum apparently occurs for $R_N > 20$ ft, whereas for the higher entry velocities considered, the optimum R_N ranges from 1.5 to 0.4 ft.

Consider next the results obtained with the incident radiation heating reduced to $q_R/2$. At very small R_N, the total heat flux is convection-dominated, and the reduction in q_{r_w} has little effect, but at large R_N, the incident radiation dominates,

Table 3 Radiative fluxes from an adiabatic shock layer

R_N, ft	δ, ft	Radiation fluxes, Btu/sec-ft^2 Continuum	Line	Total
	h_∞ = 220 kft, V_∞ = 35,000 fps			
0.01	0.000441	0.3	1.7	2.0
10.0	0.441	103.5	87.1	190.6
	h_∞ = 220 kft, V_∞ = 55,000 fps			
0.01	0.000409	10.6	50.0	60.6
10.0	0.409	5,712	3,563	9,275
	h_∞ = 190 kft, V_∞ = 35,000 fps			
0.01	0.000459	1.7	8.4	10.1
10.0	0.459	449	409	858
	h_∞ = 190 kft, V_∞ = 55,000 fps			
0.01	0.000430	85.5	294.1	379.6
10.0	0.430	24,220	12,890	37,110

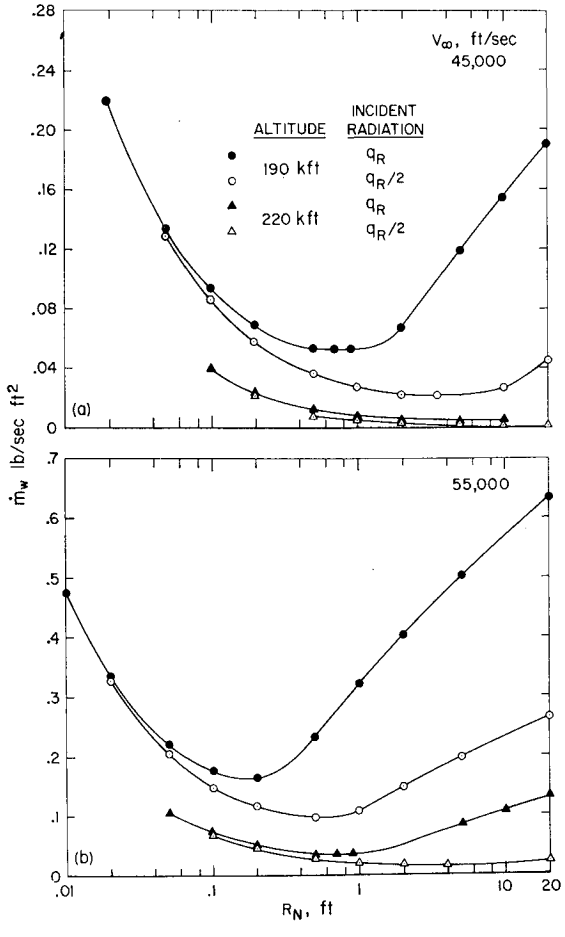

Fig. 4 Graphite ablation rates.

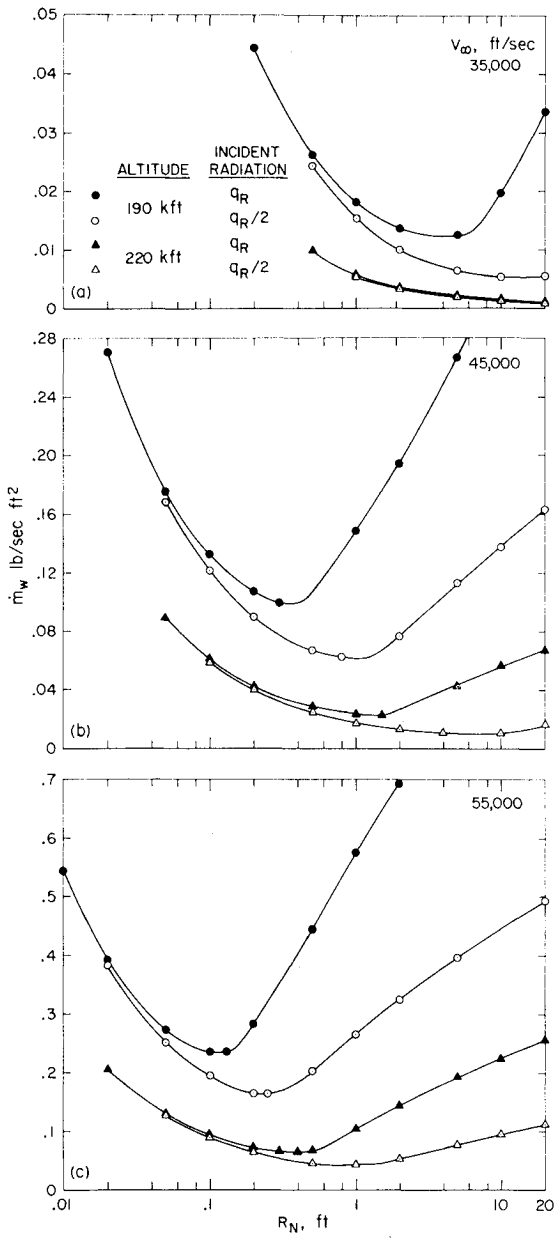

Fig. 5 Nylon-phenolic ablation rates.

so that $\dot{m}_w \propto q_{r_w}$ [see Eq. (1)]. This is demonstrated by the results for nylon-phenolic at 55 kft/sec and 190 kft (Fig. 5c); at $R_N = 2$ ft, the reduction of the incident radiation heating from q_R to $q_R/2$ reduces the $\dot{m}_w$ nearly proportionately, from 0.693 to 0.325 lb/sec-ft².

At intermediate R_N, the effect on $\dot{m}_w$ of decreasing q_{r_w} can be nearly monotonic between these two limiting cases. As an example, this happens for the flight conditions and material just cited. However, in several cases the reduction of q_{r_w} by a factor of two yields a much more substantial decrease in $\dot{m}_w$. For example, a sixfold reduction in $\dot{m}_w$ is obtained for graphite at 45 kft/sec, 190 kft, and R_N of 10 ft (Fig. 4a) and nylon-phenolic at 35 kft/sec, 190 kft and R_N of 20 ft (Fig. 5a). This latter situation occurs when the reduction in q_{r_w} is such as to produce a sizable increase in the fraction of the total heating rate which is reradiated from the surface.

In either event, halving q_{r_w} tends to decrease the minimum $\dot{m}_w$, by a factor ranging from 0.70 for nylon-phenolic at 55 kft/sec and 220 kft to 0.40 for graphite at 45 kft/sec and 190 kft. Moreover, the reduction in q_{r_w} from q_R to $q_R/2$ causes the minimum $\dot{m}_w$ to occur at a larger R_N, by a factor ranging from 2.0 for nylon-phenolic at 55 kft/sec and 190 kft to 6.7 for graphite at 55 kft/sec and 220 kft, and produces near-minimum ablation over a much wider range of R_N.

Considering the nylon-phenolic results for 190 kft altitude, q_R, and V_∞'s of 35, 45, and 55 kft/sec, it is apparent that any R_N from 1 in. to 20 ft or more is satisfactory for the 35 kft/sec condition, but that an R_N larger than a few inches yields a 3- to 5-fold increase in $\dot{m}_w$ at the 55 kft/sec condition. For $q_R/2$, an R_N larger than a few inches yields only a 2- to 3-fold increase in $\dot{m}_w$ at $V_\infty = 55$ kft/sec. The significance of R_N will be discussed further in an example calculation for a representative 50 kft/sec re-entry trajectory.

Heating Rates

Figure 6a shows that, for the four materials considered for a given flight condition, the convective heating rate is reduced to zero for R_N's slightly larger than those for minimum ablation (e.g., for nylon-phenolic, q_{a_w} is reduced to zero at $R_N = 0.5$ ft, while minimum $\dot{m}_w$ occurs for R_N between 0.3 and 0.4 ft—see Fig. 5b). The q_{a_w} to a nonablating wall also is shown in Fig. 6a for comparison. It is apparent that q_{a_w} for a given R_N is reduced most for teflon and least for graphite due to the higher and lower $\dot{m}_w$'s, respectively.

Figure 6b shows total heating rates for the same flight condition. It can be seen by comparing these results with the corresponding results in Figs. 4 and 5 that the total heating rate tends to have a less pronounced minimum with R_N, and that minimum ablation occurs at a slightly larger R_N (e.g., the minimum ablation for nylon-phenolic occurs for R_N between 0.3 and 0.4 ft, while the minimum total heating occurs for R_N between 0.2 and 0.3 ft. The reason for this latter behavior is that T_w (and, hence, q_{rerad} and h_w) continue to rise as R_N is increased beyond that for minimum total heating [see Eq. (1)].

A significant result is that reradiation can be very important or relatively unimportant depending upon the particular material and flight condition. This has already been mentioned as the reason for strikingly different ablation behavior when q_{r_w} is reduced by a factor of two. For example, in the case of nylon-phenolic at 190 kft altitude and incident radiation q_R, 16% or less of the incident total heating is reradiated at 55 kft/sec; 29% at 45 kft/sec; and 75% at 35 kft/sec, respectively. This fraction is increased to 97% for the high-altitude, low-V_∞ case. Thus, surface emittance (taken to be 0.65 for nylon-phenolic) is a very important material property for 35 kft/sec entry, but becomes of increasingly less significance as V_∞ is increased.

Surface Temperature

Predicted T_w's range from 6100 to 7400°R for graphite, 4600, to 6000°R for nylon-phenolic and the Apollo material, and 1740 to 2060°R for teflon. It should be kept in mind that the surface material may not be capable of surviving to these high temperatures, especially in the case of graphite, in which case actual $\dot{m}_w$'s could be considerably higher than those predicted in the present study, which considered only thermochemical ablation effects and neglected the possibility of bulk material failure.

Transfer-Coefficient Correlations

It is useful to seek a correlation of the convective heat- and mass-transfer results so as to eliminate the need for further boundary-layer solutions in future studies. Convective heat-transfer rates q_{a_w} and diffusive mass fluxes j_{k_w} are often expressed in terms of heat- and mass-transfer coefficients,[3] re-

spectively, defined by††

$$\rho_e u_e C_H \equiv q_{a_w}/(H_e - h_w) \quad (4)$$

$$\rho_e u_e C_M = \rho_e u_e C_{M_k} \equiv j_{k_w}/(\tilde{K}_{k_e} - \tilde{K}_{k_w}) \quad (5)$$

where $\tilde{K}_k$ is the mass fraction of element k irrespective of molecular configuration. These coefficients normalized by $\rho_e u_e C_{H_0}$ (the heat-transfer coefficient to a nonablating wall at the ablation temperature) are presented in Fig. 7 in terms of the conventional parameter $B_0' \equiv \dot{m}_w/\rho_e u_e C_{H_0}$. The $\rho_e u_e C_{H_0}$ values were obtained by a series of stagnation-point air solutions and are presented in Ref. 19.

Figure 7 contains the results of all of the boundary-layer solutions generated during the course of this study (each data point corresponding to one or more boundary-layer solutions) except for those results for $B_0' > 3.0$, for which $\rho_e u_e C_M$ and $\rho_e u_e C_H$ are essentially zero. They thus represent solutions for wide ranges of total enthalpy (24,000 to 60,000 Btu/lb) and pressure (0.2 to 1.1 atm), as well as R_N, T_w, ratios of convective to radiative heating rates, and the like. In view of this, the transfer coefficients correlate extremely well, the deviation of $\rho_e u_e C_H$ or $\rho_e u_e C_M$ for any given boundary-layer solution from the single-curve correlation for that material seldom exceeding 0.5% of $\rho_e u_e C_{H_0}$.

The molecular weights of the gas mixture adjacent to the wall range between 84 and 98 for teflon, 28 and 30 for graphite, 22 and 17 for the Apollo material, and 22 and 14 for nylon-phenolic, with the second figure in each case being representative of very large blowing rates where the wall gas is principally injectant with little air dilution. The C_M/C_{H_0} ratios vary monotonically with the injectant molecular weight. The C_H/C_{H_0} behavior is not as well ordered, but fortunately the effect of molecular weight is relatively small: a single curve could be drawn which would represent all of the solutions with the exception of teflon within 2% of $\rho_e u_e C_{H_0}$. Therefore, one would probably not be too far wrong if he were to guess the transfer-coefficient behavior for another material such as carbon-phenolic on the basis of injectant molecular weight or molecular weight of the wall gas.

Prediction Procedures

The present results can be used to generate predictions for $\dot{m}_w$'s by one of the following three methods:

1) A rapid estimate of $\dot{m}_w$'s can be obtained directly from Fig. 4 or 5 using either q_R or $q_R/2$, or using the reader's preference for q_{r_w} (corrected for ablation-products absorption, if desired), in which case it is necessary to interpolate between the q_R and $q_R/2$ results.‡‡

2) Detailed solution to the energy balance, Eq. (1), can be obtained to yield accurate estimates of $\dot{m}_w$ and T_w using the transfer-coefficient correlations of Fig. 7, again for any desired incident radiation heating model. Two additional pieces of information are required, however, namely $B' \equiv \dot{m}_w/\rho_e u_e C_M$ and h_w as functions of T_w and P. These have been generated as part of the coupled boundary-layer solutions reported in this paper and are presented in Ref. 19. This information can also be generated with a surface thermochemical ablation program such as that described in Refs. 3 and 16. This latter approach has been done for graphite and nylon-phenolic for pressures of 0.1 and 1.0 atm and the results are presented in Table 4. An iterative solution of the surface energy balance can be performed by hand,[19] or machine calculations can be performed for transient as well as steady-state conditions using computer codes described in Ref. 16.

3) Method 2 above could be used to generate a comprehensive set of $\dot{m}_w$ design charts for a particular radiation model. A particularly convenient form would be $\dot{m}_w$ vs V_∞ with altitude as a parameter for various R_N's of potential interest. These charts could then be applied directly to a specific trajectory with a much higher degree of accuracy than is possible with the present Figs. 4 and 5 and much more rapidly than by direct use of Method 2 above.

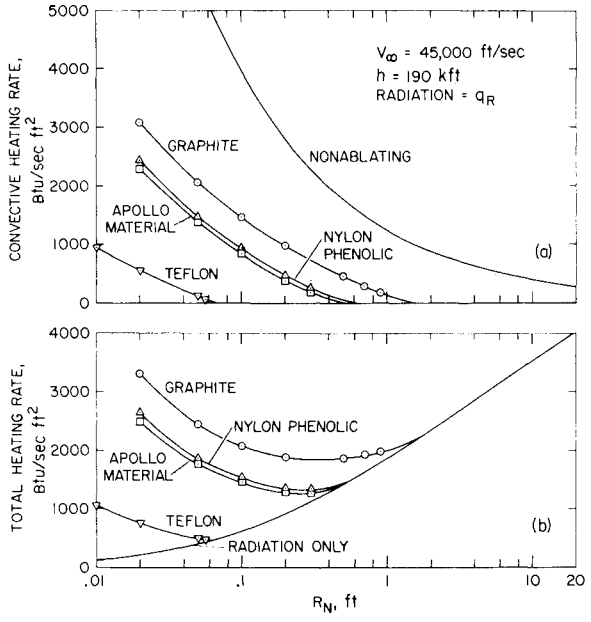

Fig. 6 Convective and total heating rates for various ablation materials.

Application of Method 2

The hand iteration procedure was applied to the Apollo material§§ subjected to the representative 50 kft/sec trajectory shown in Fig. 8a; $\dot{m}_w$ histories for R_N's of 0.1, 1.0, and 10.0 ft are presented in Fig. 8b for incident radiation heating rates q_R. Of the three cases considered, the intermediate R_N

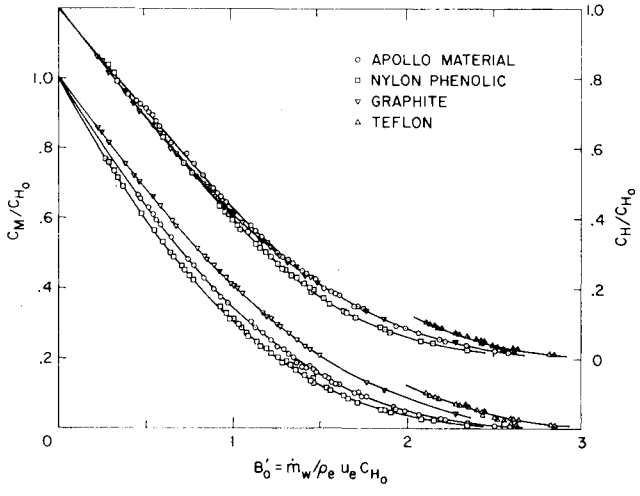

Fig. 7 Heat- and mass-transfer coefficient correlations.

†† The $\rho_e u_e C_{M_k}$ are all equal in the present solutions since diffusion coefficients are considered equal for all species.

‡‡ When considering nonspherical nose caps, the abscissa R_N of Figs. 4 and 5 should be interpreted as the "effective nose radius" of convective heating,[24] and the incident radiation heating should be calculated for the actual shock standoff distance.

§§ It is shown in Ref. 19 that the mass ablation rates for the Apollo material are slightly higher than those predicted for nylon-phenolic.

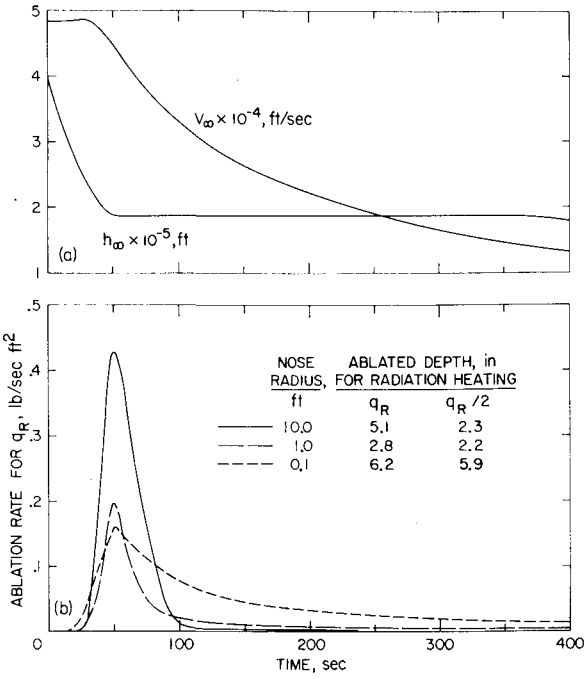

Fig. 8 Apollo material ablation for representative 50,000 fps trajectory.

is seen to yield the best ablation performance. The reason is evident from Fig. 8b: an increase of R_N to 10.0 ft yields a severe penalty in $\dot{m}_w$ near peak heating with little benefit from reduced convective heating during the constant-altitude phase, whereas a decrease of R_N to 0.1 ft yields a severe penalty in $\dot{m}_w$ due to increased q_a during the constant-altitude phase with little benefit from the decreased q_r at peak heating.

This result is intended to illustrate the use of the procedure, and should not be used to draw general conclusions regarding vehicle sizing for two reasons. First, sizing depends strongly on the specific trajectory and ablation material, and second, it is highly dependent upon the radiation model which is employed. For example, if the Ref. 2 correlation for the reduction in q_R due to ablation-products absorption is applied to the trajectory of Fig. 8a, an entirely different conclusion results. In particular, absorption by the ablation products reduces the peak $\dot{m}_w$ by 63%, 50% and 12% for R_N's of 10, 1, and 0.1 ft, respectively, and the ablated depths for the entire trajectory are decreased by 55%, 21% and 5%. Consequently, the ablated depth for R_N = 10 ft is reduced to roughly the same value as for R_N = 1 ft. Obviously, the extent to which q_R is reduced by ablation products absorption can be very important in sizing superorbital re-entry vehicles.

Summary

Results are given for the chemically-reacting stagnation-point boundary layer fully coupled to a steady-state surface ablation boundary condition. The boundary-layer profiles are considered to be unaltered by absorption of radiation by the ablation products; however, they are strongly affected indirectly by the high surface mass-transfer rates produced by the radiation heating. Incident radiation heating is treated parametrically, the baseline values being calculated using a nongray radiation model including lines. Procedures are outlined which utilize the results to estimate ablation rates for any trajectory, nose geometry, and incident radiation model, which can be corrected for radiation cooling and ablation-products absorption.

It is seen that vehicle sizing is strongly dependent upon the particular material, trajectory, and net radiation flux to the surface. In particular, the extent to which the ablation products reduce the incident convective and radiative heating is of paramount importance. Correlations for the former which are based on the present boundary-layer solutions are presented which permit accurate representation of convective heating all the way to boundary-layer blowoff. Some results for the latter can be found in the literature, but much more work needs to be done in this area before firm conclusions can be made regarding vehicle sizing.

Finally, the results demonstrate that vehicle sizing should be based on ablation rate rather than total heating (incident radiation plus convection) such as is normally done, because an increase in total heating by a factor of two can produce a six-fold increase in ablation rate due to the relatively smaller fraction of energy which can be reradiated.

Table 4 Blowing parameters and wall gas enthalpies

P = 0.1 atm			P = 1.0 atm		
T_w, °R	B'	h_w, Btu/lb	T_w, °R	B'	h_w, Btu/lb
Graphite					
3600	0.1764	276	3600	0.1764	276
4500	0.1765	554	4500	0.1764	553
5400	0.1839	918	5400	0.1782	855
5850	0.2304	1540	5850	0.1867	1090
6300	0.5624	4238	6300	0.2289	1664
6449	1.000	6349	6750	0.4273	3478
6570	2.000	8842	7200	1.823	8736
6663	5.000	11324	7342	5.000	11562
6701	10.00	12450	7393	10.00	12705
6730	30.00	13321	7431	30.00	13592
6741	100.00	13652	7446	100.0	13931
6747	∞	13799	7453	∞	14082
Nylon-phenolic					
3600	0.3095	457	3600	0.3095	450
4500	0.3458	1058	4500	0.3450	948
5400	0.7036	3399	5400	0.5220	2141
5631	2.000	6273	5850	1.519	4730
5700	5.000	8096	5978	5.000	6876
5723	10.00	8924	6007	10.00	7580
5739	30.00	9569	6027	30.00	8128
5745	100.0	9817	6035	100.0	8339
5748	∞	9927	6038	∞	8433

References

[1] Bartlett, E. P. et al., "Improved Heat-Shield Design Procedures for Manned Entry Systems II. Application to Apollo," Rept. 70-15, Pt. II, June 1970, Aerotherm Corp., Mountain View, Calif.

[2] Coleman, W. D. et al., "A Study of the Effects of Environmental and Ablator Performance Uncertainties on Heat Shielding Requirements for Blunt and Slender Hyperbolic-Entry Vehicles," AIAA Paper 68-154, New York, 1968.

[3] Kendall, R. M., Rindal, R. A., and Bartlett, E. P., "A Multicomponent Boundary-Layer Chemically Coupled to an Ablating Surface," *AIAA Journal*, Vol. 5, No. 6, June 1967, pp. 1063–1071.

[4] Anderson, J. D., Jr., "An Engineering Survey of Radiating Shock Layers," *AIAA Journal*, Vol. 7, No. 9, Sept. 1969, pp. 1665–1675.

[5] Chin, J. H., "Radiation Transport for Stagnation Flows Including Effects of Lines and Ablation Layer," *AIAA Journal*, Vol. 7, No. 7, July 1969, pp. 1310–1318.

[6] Callis, L. B., "Time Asymptotic Solutions of Blunt-Body Stagnation-Region Flows with Nongray Emission and Absorption of Radiation," AIAA Paper 68-663, Los Angeles, Calif., 1968.

[7] Wilson, K. H. and Hoshizaki, H., "Effect of Ablation Product Absorption and Line Transitions on Shock Layer Radiative Transport," NASA CR-1264, Feb. 1969, Lockheed Missiles & Space Co., Palo Alto, Calif.

[8] Page, W. A. et al., "Radiative Transport in Inviscid Nonadiabatic Stagnation-Region Shock Layers," AIAA Paper 68-784, Los Angeles, Calif., 1968.

[9] Rigdon, W. S., Dirling, R. B., Jr., and Thomas, M., "Radiative and Convective Heating During Atmospheric Entry," DAC-60913, March 1968, Douglas Aircraft Co., MSSD, Santa Monica, Calif.

[10] Olstad, W. B., "Correlations for Stagnation-Point Radiative Heat Transfer," *AIAA Journal*, Vol. 7, No. 1, Jan. 1969, pp. 170–172.

[11] Nicolet, W. E., "Advanced Methods for Calculating Radiation Transport in Ablation-Product Contaminated Boundary Layers," NASA CR-1656, Sept. 1970, Aerotherm Corp., Mountain View, Calif.

[12] Hoshizaki, H. and Lasher, L. E., "Convective and Radiative Heat Transfer to an Ablating Body," *AIAA Journal*, Vol. 6, No. 8, Aug. 1968, pp. 1441–1449.

[13] Kendall, R. M. and Bartlett, E. P., "Nonsimilar Solution of the Multicomponent Laminar Boundary Layer by an Integral-Matrix Method," *AIAA Journal*, Vol. 6, No. 6, June 1968, pp. 1089–1097.

[14] Bartlett, E. P. and Kendall, R. M., "Nonsimilar Solution of the Multicomponent Laminar Boundary Layer by an Integral-Matrix Method," NASA CR-1062, June 1968, Aerotherm Corp., Mountain View, Calif.

[15] Anderson, L. W. and Kendall, R. M., "A Nonsimilar Solution for Multicomponent Reacting Laminar and Turbulent Boundary Layer Flows Including Transverse Curvature," AFWL-TR-69-106, Oct. 1969, Aerotherm Corp., Mountain View, Calif.

[16] Bartlett, E. P. et al., "Further Studies of the Coupled Chemically Reacting Boundary Layer and Charring Ablator," NASA CR-92471, Oct. 1968, Aerotherm Corp., Mountain View, Calif.

[17] Deblaye, C. and Bartlett, E. P., "An Evaluation of Thermodynamic and Transport Properties for Use in the BLIMP Nonsimilar Multicomponent Boundary-Layer Program," Sandia SC-CR-69-3271, July 1969, Aerotherm Corp., Mountain View, Calif.

[18] Hirschfelder, J. O., Curtiss, C. F., and Bird, R. B., *Molecular Theory of Gases and Liquids*, 2nd Printing, corrected, with notes added, Wiley, New York, 1964.

[19] Bartlett, E. P., Nicolet, W. E., and Howe, J. T., "Heat-Shield Ablation at Superorbital Reentry Velocities," Rept. 69-63, Dec. 1969, Aerotherm Corp., Mountain View, Calif.

[20] Kendall, R. M., "A General Approach to the Thermochemical Solution of Mixed Equilibrium-Nonequilibrium, Homogeneous or Heterogeneous Systems," NASA CR-1064, June 1968, Aerotherm Corp., Mountain View, Calif.

[21] Hayes, W. D. and Probstein, R. F., *Hypersonic Flow Theory, Inviscid Flows*, 2nd ed., Vol. 1, Academic Press, New York, 1966.

[22] Woodward, H. T., "Predictions of Shock-Layer Radiation from Molecular Band Systems in Proposed Planetary Atmospheres," TN D-3850, 1967, NASA.

[23] Biberman, L. M., Mnatsakanyan, A. Kh., "Optical Properties of Air in the Temperature Range from 4,000 to 10,000°K," *Teplofizika Vysokikh Temperatur*, Vol. 4, No. 2, March-April 1966, pp. 148–159.

[24] Boison, J. C. and Curtiss, H. A., "An Experimental Investigation of Blunt Body Stagnation Point Velocity Gradient," *ARS Journal*, Vol. 29, No. 2, Feb. 1959, pp. 130–135.

MAY 1971 J. SPACECRAFT VOL. 8, NO. 5

An Evaluation of Ablation Mechanisms for the Apollo Heat Shield Material

EUGENE P. BARTLETT* AND LARRY W. ANDERSON†
Aerotherm Corporation, Mountain View, Calif.

AND

DONALD M. CURRY‡
NASA Manned Spacecraft Center, Houston, Texas

Theoretical ablation solutions for the Apollo heat shield material are compared with data obtained in an arc-plasma tunnel. Some of the more important parameters considered are pyrolysis gas reactivity with the boundary-layer gases, changes in surface elemental composition due to in-depth coking reactions, mechanical removal of candidate surface species, loss of pyrolysis gas through fissures which are seen experimentally to develop in the chars, and surface thermochemistry including silica-carbon reactions. Chemical ablation theory is satisfactory at moderately high surface temperatures if it is assumed that the pyrolysis gases are not effective in blocking the convective heat transfer. At lower surface temperatures, it is necessary to employ a rate law for the mechanical removal of silica in the char material.

Nomenclature

B_c' = char recession rate normalized by $\rho_e u_e C_M$
B_g' = pyrolysis gas rate normalized by $\rho_e u_e C_M$
P = pressure
$\dot{S}$ = linear surface recession rate
T_F, T_w = fail temperature and surface temperature
X = mole fraction
ρ_c, ρ_g = densities of char and pyrolysis gas
$\rho_e u_e C_M$ = mass-transfer coefficient

Subscript

c = condensed phase (on chemical element or molecule)

Presented as Paper 69-98 at the AIAA 7th Aerospace Sciences Meeting, New York, January 20–22, 1969; submitted February 11, 1969; revision received January 11, 1971. This work was supported by the NASA Manned Spacecraft Center, Structures and Mechanics Division, under Contract NAS9-6719.

* Manager, Applied Research Department. Member AIAA.
† Staff Engineer, Applied Research Department. Member AIAA.
‡ Aerospace Engineer. Thermal Technology, Structures and Mechanics Division.